Embedding Fe(0) electrocoagulation in a biologically active As(III) oxidising filter bed

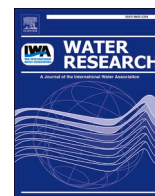Roy, Mrinal; Kraaijeveld, Erik; Gude, Jink C. J . ; van Genuchten, Case M.; Rietveld, Luuk C.; van Halem, Doris

Important note
To cite this publication, please use the final published version (if applicable).
Please check the document version above.

Contents lists available at ScienceDirect

Water Research

Embedding Fe(0) electrocoagulation in a biologically active As(III) oxidising filter bed

Mrinal Roy [a,*], Erik Kraaijeveld [a], Jink C . J . Gude [b], Case M. van Genuchten [c], Luuk C. Rietveld [a], Doris van Halem [a]

[a] Water Management Department, Faculty of Civil Engineering and Geosciences, Delft University of Technology, Stevinweg 1, 2628CN Delft, the Netherlands
[b] NX Filtration BV, Josink Esweg 44, 7545PN Delft, the Netherlands
[c] Department of Geochemistry, Geological Survey of Denmark and Greenland, Copenhagen DK-1350, Denmark

ARTICLE INFO

ABSTRACT

Long-term consumption of groundwater containing elevated levels of arsenic (As) can have severe health consequences, including cancer. To effectively remove As, conventional treatment technologies require expensive chemical oxidants to oxidise neutral arsenite (As(III)) in groundwater to negatively charged arsenate (As(V)), which is more easily removed. Rapid sand filter beds used in conventional aeration-filtration to treat anaerobic groundwater can naturally oxidise As(III) through biological processes but require an additional step to remove the generated As(V), adding complexity and cost. This study introduces a novel approach where As(V), produced through biological As(III) oxidation in a sand filter, is effectively removed within the same filter by embedding and operating an iron electrocoagulation (FeEC) system inside the filter. Operating FeEC within the biological filter achieved higher As(III) removal (81 %) compared to operating FeEC in the filter supernatant (67 %). This performance was similar to an analogous embedded-FeEC system treating As(V)-contaminated water (85 %), confirming the benefits of incorporating FeEC in a biological bed for comparable As(III) and As(V) removal. However, operating FeEC in the sand matrix consumed more energy (14 Wh/m^3) compared to FeEC operated in a water matrix (7 Wh/m^3). The efficiency of As removal increased and energy requirements decreased in such embedded-FeEC systems by deep-bed infiltration of Fe(III)-precipitates, which can be controlled by adjusting flow rate and pH. This study is one of the first to demonstrate the feasibility of embedding FeEC systems in sand filters for groundwater arsenic removal. Such systems capitalise on biological As(III) oxidation in aeration-filtration, effectively eliminating As(V) within the same setup without the need for chemicals or major modifications.

1. Introduction

To minimise the potential health risks associated with elevated levels of arsenic (As) in groundwater, it is crucial to treat the water before consumption. Exposure to such contaminated water has been linked to various cancers, including skin, lung, prostate, and kidney cancer, as well as neurodevelopmental issues in children (Kapaj et al., 2006; Sodhi et al., 2019; Steinmaus et al., 2014). Consequently, the World Health Organization (WHO) has established a provisional guideline value of less than 10 μg/L As in drinking water (WHO, 2004).

Extensive research has been conducted on various standard technologies, such as adsorption, coagulation, precipitation, and filtration, to address the removal of arsenic (As) from groundwater (Alka et al.,

2021; Kowalski, 2014). However, these methods often face limitations in terms of their efficacy, primarily due to the oxidation state of As. In raw anaerobic groundwater, As exists as neutrally charged arsenite (As (III)) (H$_3$AsO$_3$), which is more difficult to remove compared to the oxidised form, arsenate (As(V)), a negatively charged oxyanion at neutral pH (H$_2$AsO$_4^-$/HAsO$_4^{2-}$) (Roberts et al., 2004).

While aeration is commonly employed after extracting raw anaerobic groundwater, the oxidation of As(III) to As(V) through aeration (i. e., oxidation by molecular oxygen) at near-neutral pH is a slow process, taking several days for completion (Hug and Leupin, 2003). Consequently, to enhance the removal of As(III) using the aforementioned technologies, pre-oxidation to As(V) using strong chemical oxidants like NaOCl and KMnO$_4$ has been reported (Ahmad et al., 2018; Sorlini and

Gialdini, 2010). However, the use of chemical oxidants increases costs, can lead to operational difficulties, and generates unwanted by-products that necessitate additional treatment (Jackman and Hughes, 2010; Katsoyiannis and Zouboulis, 2004).

Other studies have proposed a chemical-free approach to achieve effective oxidation of As(III) during conventional aeration-filtration by employing arsenic-oxidising bacteria (AsOB) to biologically oxidise As (III) (Gude et al., 2018c; Katsoyiannis and Zouboulis, 2004; Lytle et al., 2007). Long-term exposure of rapid sand filter (RSF) beds to As (III)-contaminated water leads to the development and accumulation of a diverse microbial community, including AsOB, which effectively oxidise As(III) throughout the filter bed depth (Gude et al., 2018c; Roy et al., 2020). Additionally, aeration-filtration is commonly employed to remove native-Fe(II) from groundwater by oxidising it to form Fe (III)-precipitates, which can potentially adsorb the oxidised As(V) and remove it during this treatment step. However, complete biological As (III) oxidation predominantly occurs at a specific depth within the filter bed (around 40–60 cm from the top layer) (Gude et al., 2018a, 2018b; Yang et al., 2014), where the Fe(III)-precipitates have already been removed and are unavailable for adsorption of As(V) (Gude et al., 2018a, 2018b). Therefore, additional dosing of Fe is necessary to remove the biologically oxidised As(V) after aeration-filtration.

Iron-electrocoagulation (FeEC) is a chemical-free method that can be employed to introduce Fe into water and remove the oxidised As(V), as demonstrated in numerous studies focusing on treating As-contaminated water (Amrose et al., 2014; Bandaru et al., 2020; Delaire et al., 2017; Mollah et al., 2004). In FeEC, an electric current is passed through Fe(0) electrodes, releasing Fe(II) ions from the sacrificial Fe(0) anode into the solution. These Fe(II) ions can be oxidised by dissolved oxygen (DO) to produce Fe(III)-precipitates with a high affinity for adsorbing As (van Genuchten et al., 2012). Various forms of Fe(III)-precipitates, ranging from poorly-ordered hydrous ferric oxides to crystalline magnetite, have been observed during FeEC, with As being either adsorbed or incorporated into the solid structure (van Genuchten et al., 2012, 2014, 2019, 2020). However, conventional FeEC has primarily been applied in a water matrix. Therefore, to harness the benefits of biological As(III) oxidation in conventional aeration-filtration, FeEC should be positioned post-filtration, allowing oxidation to occur within the filter bed. The conventional approach would involve applying FeEC to the filtrate of the biological bed, followed by an additional filtration step to remove the As-laden Fe(III)-precipitates, which would require constructing additional infrastructure. By contrast, an ideal system would utilise a single integrated reactor to couple both biological As(III) oxidation and Fe(III) production via FeEC. Such a system could be achieved by embedding and operating FeEC within the biological sand filter to generate and filter Fe within a single system. However, to the best of our knowledge, embedding FeEC has only recently been investigated for As removal in soils and has not been studied in the context of a sand filter (Kumpiene et al., 2023). Examining embedded-FeEC within a sand filter is crucial for understanding key parameters, including overall As removal efficiency, energy consumption and the role of FeEC operating conditions, before implementing such a system at scale.

In this study, we evaluated three specific systems: FeEC embedded and operated inside a biotic filter bed, FeEC in the supernatant of a biotic filter bed, and FeEC embedded inside an abiotic filter bed. The performance of these different systems was compared in terms of As removal efficiency, energy consumption, and deep-bed Fe infiltration, with additional consideration of the impact of FeEC location, biological As (III) oxidation, initial As oxidation state, and operational conditions (Fe dosage, flow rate, and pH). The novelty of this work lies in effectively utilising the biological As(III) oxidation step in conventional aeration-filtration and removing the oxidised As(V) within the same filtration step, without any chemicals and major structural changes. The results from this study improve the understanding of the operation of such embedded-FeEC systems for As removal under a range of realistic conditions.

2. Materials and methods

2.1. Experimental setup

2.1.1. Batch-FeEC

The quantity of iron (Fe) released from the anode during iron-electrocoagulation (FeEC) is directly related to the charge dosage (CD) (q in C/L) and can be determined using Faraday's law (Eq. (1)) (Roy et al., 2020).

$$W = \frac{qM}{nF} = \frac{ItM}{nFV} = \frac{IM}{nFQ} \tag{1}$$

where, W = Amount of generated Fe (mg/L); I = Applied current (A); t = Electrolysis time (s); M = Molecular weight of Fe (mg/mol) = 55,845; F = Faraday's constant (96,485 C/mol); n = Number of transferred electrons (2 for Fe); V = Solution volume (L); Q = Flow rate (L/s).

To determine the appropriate CD or Fe dosage for the subsequent flow-through embedded-FeEC experiments, batch FeEC experiments were conducted. A comprehensive description of the batch FeEC reactor, operational parameters, and the obtained results can be found in the Supplementary Information (S1 and S2).

2.1.2. Column setup

The experimental setup consisted of four PVC down-flow columns, each with a height of 1.7 m and a diameter of 7.4 cm (Fig. 1(A)). These columns contained fresh anthracite, serving as the filter material, with a bed height of 80 cm. The anthracite material had a porosity of 0.43 $\pm$0.01 and a median particle size (d_{50}) of 1.9 mm. During the experiments, a supernatant water level of 20–25 cm above the anthracite bed was maintained. Prior to the experiments, the anthracite beds were thoroughly backwashed with tap water until the supernatant appeared visually clean, ensuring the removal of solids.

Two of the four columns were initially used to establish a microbial community capable of oxidising As(III) within the anthracite beds (referred to as biotic columns) (Fig. 1(B)) (further details in Section 2.2.1). Subsequently, modifications were made to the two biotic columns: one had a FeEC cell placed inside the bed (referred to as biotic embedded-FeEC), and the other had the FeEC cell placed in the supernatant water (referred to as supernatant-FeEC) (Fig. 1(C)) (further details in Section 2.2.2). A clean layer of sand (height = 40 cm; porosity = 0.40$\pm$0.01; d50 = 1.2 mm) was also added at the bottom of the biotic embedded-FeEC and supernatant-FeEC columns to enhance filtration. The remaining two columns were duplicates, with anthracite beds that were abiotic but embedded with a FeEC cell (referred to as abiotic embedded-FeEC) (Fig. 1(D)) (further details in Section 2.2.3).

The FeEC cell in all four columns consisted of two perforated Fe electrodes (anode diameter = 75 mm; cathode diameter = 55 mm; perforation diameter = 12 mm; open surface area = 51 %) (Fig. S4 and S5), connected to a DC power supply (TENMA 72–10,500 Power Supply, 30 V, 3A). The electrodes were horizontally positioned within the anthracite bed or in the supernatant water. The perforations allowed for easy placement and removal of the electrodes during backwashing of the filter bed. The anode was positioned downstream of the cathode, and an inter-electrode gap of 1.5 cm was maintained using a plastic spacer (Fig. S5). Nylon wire was used to secure the electrodes and maintain a consistent configuration throughout the experiment. Before and after the FeEC operation, backwashing was performed with tap water to achieve a visually clean supernatant (approximately 15 min before and 30 min after FeEC operation), resulting in a bed expansion of 25–30 %. During these backwashing periods, the electrodes were lowered into and removed from the fluidised bed. Prior to placement, the electrodes were cleaned following the procedure described in the batch study (S1). When the FeEC cell was not operational, the electrodes were kept dry outside the columns. Sample points were located on the sides of the columns, corresponding to different heights within the bed.
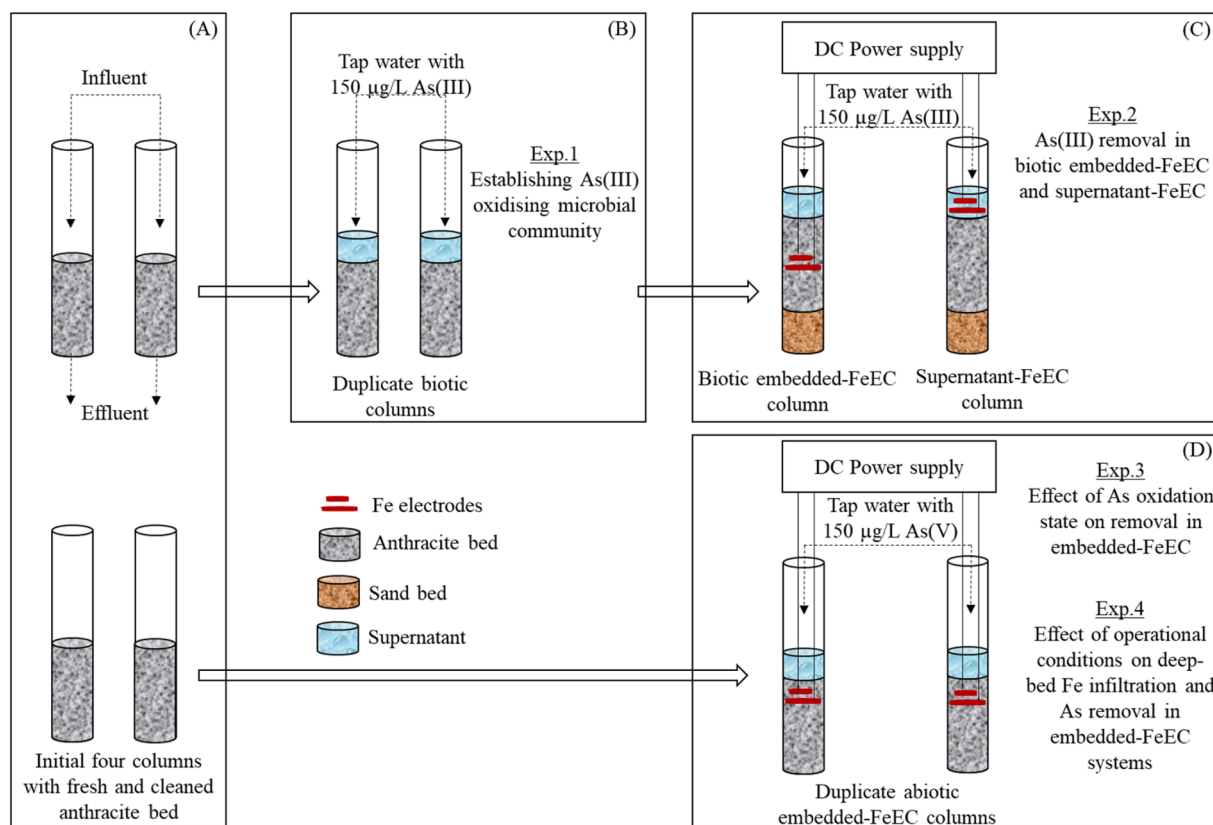
Fig. 1. Schematic diagram of the different columns used and overview of the experiments performed during this study.

2.2. Overview of column experiments

2.2.1. Establishing As(III) oxidising microbial community

The procedure for establishing an As(III)-oxidising biomass on a sand bed resembled the methodologies outlined in the previous studies by Gude et al. (2018c), and Roy et al. (2020). These studies focused on the establishment and characterisation of AsOB in sand filters for biological As(III) oxidation. To establish an As(III)-oxidising biomass, the two biotic filter columns were subjected to a nine-week ripening period with 150 μg/L As(III)-spiked tap water flowing at a rate of 3 m/h (Fig. 1(B)). During this period, aluminium foil was wrapped around the columns to shield the filter material from light exposure. The pH of the water was consistently maintained at 7.9±0.1 using HNO_3 acid, which was the pH of the tap water used in this study (Table S2). The extent of biological As (III) oxidation within the columns was assessed on a weekly basis by analysing the speciation of dissolved As in the influent and effluent (speciation procedure in Section 2.4). Once the microbial biomass in the filter beds had been established, capable of oxidising over 95 % of the influent 150 μg/L As(III) in the effluent (after nine weeks), an As(III) oxidation profile across the bed height was obtained to determine the optimal placement of Fe electrodes within the biological bed.

2.2.2. As(III) removal in biotic embedded- and supernatant-FeEC columns

The biotic embedded-FeEC and supernatant-FeEC columns were utilised for these experiments (Fig. 1(C)). In the biotic embedded-FeEC column, the Fe electrodes were positioned at a filter depth of 50 cm from the top of the filter bed, where 85 % of the As(III) oxidation was observed in the ripened anthracite bed during week 9. In the supernatant-FeEC column, the Fe electrodes were placed in the supernatant water, 15 cm above the top of the bed.

To assess and compare the removal of As(III) in the two columns, tap water spiked with 150 μg/L As(III) was fed into both columns at a flow rate of 3 m/h, pH of 8.0, and FeEC operated at a CD of 6.4 C/L (or $I =$

0.022 A as per Eq. (1)). The CD value was determined based on the batch-FeEC experiments (S2). The two columns were operated continuously for three consecutive days, with FeEC operated for 11 h each day. Water samples were collected from the influent and effluent at the 7th, 9th, and 11th hour of operation. At the 11th hour, additional samples were collected at depths of 40 cm and 80 cm from the top of the bed to obtain As and Fe oxidation/removal profiles, followed by a backwashing step. After 11 h of FeEC operation and backwashing, the columns were flushed with tap water (without As) until the subsequent trial, which occurred approximately 12 h later, to minimise the impact of As desorption from the filter bed.

2.2.3. Effect of As oxidation state on removal in embedded-FeEC systems

To investigate the influence of the As oxidation state on the performance of embedded-FeEC and the potential advantages of embedding FeEC in a biological bed for As(III) removal, a separate set of experiments were conducted using As(V)-spiked tap water. In these experiments, the duplicate abiotic embedded-FeEC columns were utilised, with the Fe electrodes embedded 10 cm from the top of the abiotic anthracite bed (Fig. 1(D)). Both columns were operated with tap water spiked with 150 μg/L As(V), while maintaining similar pH, flow rate, and CD as the biotic embedded-FeEC column (Section 2.2.2). Consequently, the abiotic embedded-FeEC columns served as control, and the results were then compared to As(III) removal in the biotic embedded-FeEC column (Section 2.2.2). The experiments were carried out continuously for three consecutive days, with FeEC operated for 7 h each day. Water samples were collected from the influent and effluent at the 4th, 5th, 6th, and 7th hour of operation. At the 7th hour, additional samples were collected at depths of 20 cm, 40 cm, and 60 cm from the top of the bed to obtain As and Fe oxidation/removal profiles, followed by the backwashing procedure.

2.2.4. Effect of operational conditions on deep-bed Fe infiltration and As removal in embedded-FeEC systems

Since the distribution of Fe(III)-precipitates deep within the sand filter can increase As removal, experiments were conducted to investigate the effects of charge dosage (CD), flow rate, and pH on the infiltration of Fe(III)-precipitates within the embedded-FeEC systems and its impact on As removal. The duplicate abiotic embedded-FeEC columns (Fig. 1(D)) were utilised for these experiments, operating under different conditions compared to the reference condition in Section 2.2.3 (CD = 6.4 C/L, flow rate = 3 m/h, pH = 8.0). The columns were run under modified conditions by either increasing the CD to 9.4 C/L (higher CD), increasing the flow rate to 5 m/h (higher flow rate), or lowering the pH to 7.0 (using HNO$_3$). The Fe and As depth profiles obtained during these experiments with varying operational conditions were then compared to the reference condition described in Section 2.2.3. The experimental duration, sampling procedures, and other protocols were consistent with those of the reference condition in Section 2.2.3.

2.3. Energy consumption

The energy consumption in the embedded- and supernatant-FeEC columns was estimated by monitoring the cell potential (E) and the applied current (I) during the experimental period and represented per unit of water treated, see Eq. (2).

$$\text{Energy consumption } (\text{Wh}/\text{m}^3) = mV + \frac{EI}{Q} \tag{2}$$

where m = Rate of increase in energy consumption per unit of treated water (Wh/m^3/L); V = Volume of treated water (L); EI/Q = Initial energy consumption (Wh/m^3) at the start of the experiment; E = Total cell potential (V); I = Applied current (A); Q = Flow rate (m^3/h).

2.4. Used water, chemicals, sampling and analytical methods

Chlorine-free Dutch tap water was used in all experiments, and its composition can be found in Table S2. To introduce As(III)/As(V) into the tap water, stock solutions were freshly prepared by dissolving sodium (meta)arsenite (NaAsO$_2$) or sodium arsenate dibasic heptahydrate (Na$_2$HAsO$_4$·7H$_2$O) from Sigma-Aldrich in ultrapure water. Ultrapure nitric acid (ROTIPURAN Ultra 69 %) was employed for pH adjustment, and the pH levels were monitored using a WTW SenTix 940 pH meter.

Water samples were collected for analysis in triplicate using three different methods: (a) unfiltered, (b) filtered through a 0.20 μm polystyrene sulfone filter from Macherey-Nagel GmbH & Co. KG, and (c) filtered through a 0.20 μm polystyrene sulfone filter followed by an anion exchange resin. All three types of samples were acidified with ultrapure nitric acid (ROTIPURAN® Ultra 69 %) and stored at 4 °C before analysis. The speciation of dissolved As (i.e., As(III) and As(V)) was determined using an anion exchange resin (Amberlite* IRA-402 chlorite form resin) following the method described by Gude et al. (2018c). In the case of column samples, the Fe concentration after filtration with a 0.20 μm polystyrene sulfone filter was considered as dissolved Fe (or Fe(II)), while the difference in Fe concentration between the unfiltered and 0.20 μm polystyrene sulfone filtered samples represented particulate Fe (Fe solids that were not retained by the filter bed). As and Fe concentrations were analysed using inductively coupled plasma mass spectrometry (ICP-MS) with an Analytik Jena PlasmaQuant MS instrument. The values presented in the graphs in the "Results and discussions" section represent the average of the collected water samples for each data point, and the error bars indicate the corresponding standard deviation.

3. Results and discussions

3.1. Ripening of biotic columns

Fig. S3 illustrates the As speciation in the effluent of the duplicate biotic columns (Fig. 1(B)) after being ripened with 150±20 μg/L As(III)-spiked tap water for nine weeks before their modification into the biotic embedded- and supernatant-FeEC columns. Throughout the nine-week ripening period, the oxidation of influent As(III) began within the anthracite beds, and by the 9th week, approximately 95 % of the initial 150±20 μg/L As(III) had been converted to As(V) in the effluent (Fig. S3). This trend of As(III) oxidation within the filter bed over time aligns with previous studies that focused on the establishment and characterisation of AsOB in sand filters for biological As(III) oxidation (Gude et al., 2018b, 2018c; Roy et al., 2020). Furthermore, the As(III) speciation across the ripened anthracite bed depths in week 9 revealed that approximately 88 % of the influent As(III) had been oxidised at a depth of 40 cm (Fig. 2). This finding is consistent with earlier research indicating that biological activity is highest in the upper section of the filter bed (Gude et al., 2016, 2018c). Consequently, when assembling the biotic embedded-FeEC column (Fig. 1(C)) using one of the ripened anthracite columns, the Fe electrodes were positioned at a depth of 50 cm from the top of the filter bed.

3.2. Fe and As depth profile in biotic embedded-FeEC and supernatant-FeEC columns

The As and Fe depth profiles during the runs in the biotic embedded- and supernatant-FeEC columns, which were assembled by modifying the duplicate abiotic columns after ripening, are presented in Fig. 3(A) and (B). Both columns were operated with tap water spiked with 150±20 μg/L As (130±10 μg/L As(III)) as the influent, at a flow rate of 3 m/h, and pH of 8.0. The FeEC cell was operated at a CD of 6.4 C/L, which was determined from the batch FeEC experiments (S2).

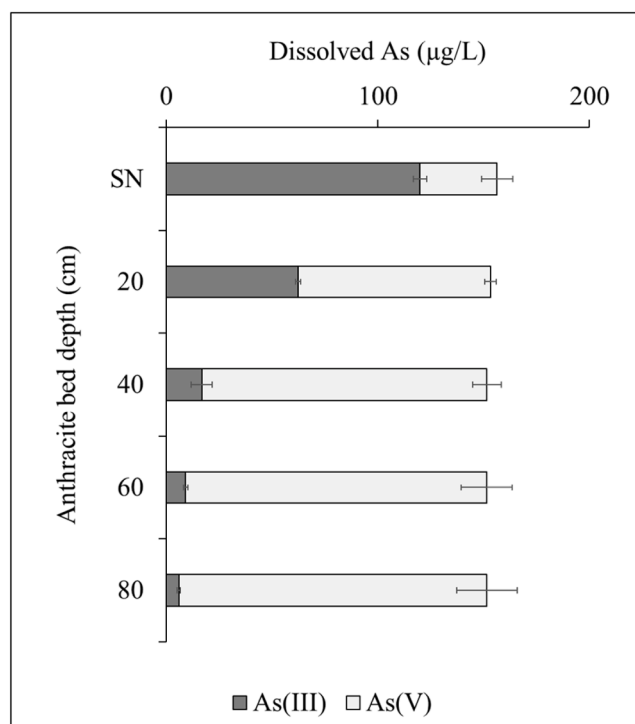The Fe profiles in both columns demonstrate that Fe generation by

Fig. 2. As(III) oxidation profile over the depth in the duplicate biotic columns after nine weeks of ripening with 150±20 μg/L As(III)-spiked tap water. SN = supernatant.

FeEC within the sand matrix was similar to conventional FeEC in a water matrix. In this process, Fe(II) was released from the anode, oxidised to Fe(III)-precipitates, and distributed across the height of the bed. In the supernatant-FeEC column, a total Fe concentration of 1.7±0.2 mg/L was measured in the supernatant water just below the FeEC cell. This released Fe corresponds to a Faradaic efficiency of approximately 1 (see eq. 1; theoretical Fe release of 1.85 mg/L), under the conditions of CD = 6.4 C/L and flow rate = 3 m/h, which aligns with literature findings (van Genuchten et al., 2018, 2017). It was assumed that a similar Fe release occurred in the biotic embedded-FeEC column (indicated by the yellow circle in Fig. 3(A)) since both systems were operated at a constant CD and flow rate. However, the actual Fe released by the embedded-FeEC could not be measured accurately due to filtration effects.

The Fe depth profiles in both columns exhibited rapid oxidation, precipitation, and filtration of the anodically-generated Fe(II). This could be attributed to the relatively high pH (8.0) and the saturated DO concentration of the solution. In the biotic embedded-FeEC column, at a bed depth of 30 cm below the FeEC cell, a dissolved Fe concentration of 0.1 mg/L and a particulate Fe concentration of 0.5 mg/L were measured, corresponding to 94 % oxidation and precipitation, as well as 67 % filtration of the released Fe(II) (considering a theoretical release of 1.85 mg/L Fe) (Fig. 3(A)). Similar trends were observed in the supernatant-FeEC column. Below the anode in the supernatant, a dissolved Fe concentration of 0.1 mg/L was measured, indicating 94 % oxidation and precipitation of the released 1.7±0.2 mg/L Fe(II). At a depth of 40 cm within the filter bed, 70 % (0.5 mg/L measured as dissolved + particulate) of the released 1.7±0.2 mg/L Fe(II) was filtered (Fig. 3(B)). These findings align with previous studies that demonstrated effective Fe removal in rapid sand filter beds (Gude et al., 2018b; Yang et al., 2014). Deeper within the bed, further oxidation and filtration of the remaining Fe were observed, which resulted in presence of only 0.2 mg/L Fe (0.1 mg/L particulate Fe) and 0.1 mg/L Fe (0.09 mg/L particulate Fe) in the effluent of the biotic embedded- and supernatant-FeEC columns, respectively. With optimisation of the filter media size, bed depth, and contact time, the removal of the remaining Fe in the effluent can be further improved.

The Fe released from the FeEC cell played a significant role in the removal of a large portion of the influent As(III) in both columns. Fig. 3 (A) and (B) illustrate the removal of the influent 150±20 μg/L As (130 ±10 μg/L As(III)) over the depth of the two columns during the experimental runs. The effluent As concentrations in the biotic embedded- and supernatant-FeEC columns were 28.9±2.5 μg/L (3.2±0.6 μg/L As (III)) and 49.1±5.3 μg/L (2.0±0.5 μg/L As(III)), respectively. This indicates that the Fe(III)-precipitates generated by FeEC effectively adsorbed and removed the As, leading to a decrease in concentration across the filter depths. However, the biotic embedded-FeEC system (81 % removal) outperformed the supernatant-FeEC system (67 % removal), with nearly double the residual As in the effluent of the supernatant-FeEC system. The higher As removal in the biotic embedded-FeEC column can be attributed to the biological oxidation of influent As(III) to As (V) in the ripened anthracite bed prior to the FeEC cell (Fig. 3(A)) (Roy et al., 2020). Fig. 3(A) demonstrates that at a depth of 40 cm, over 85 % of the influent As(III) was oxidised to As(V). Therefore, the FeEC in the biotic embedded-FeEC column (positioned at a depth of 50 cm) mainly operated in water containing As(V), which was not the case for the supernatant-FeEC column (Fig. 3(B)). The pre-oxidation of As(III) by biological processes in the biotic embedded-FeEC column resulted in a higher removal of the influent As(III), as Fe(III)-precipitates generated by FeEC have a greater affinity to adsorb As(V) than As(III) (Roberts et al., 2004). In the supernatant-FeEC column, biological oxidation of the unadsorbed As(III) was also observed in the filter bed at depths of 40 cm and 80 cm, respectively (Fig. 3(B)). However, due to insufficient remaining concentrations of Fe, the oxidised As(V) was not further removed.

3.3. Effect of As oxidation state on removal in embedded-FeEC

To further validate the improved As(III) removal in the biotic embedded-FeEC column (Section 3.2) and study the influence of As oxidation state on the removal performance of the embedded-FeEC
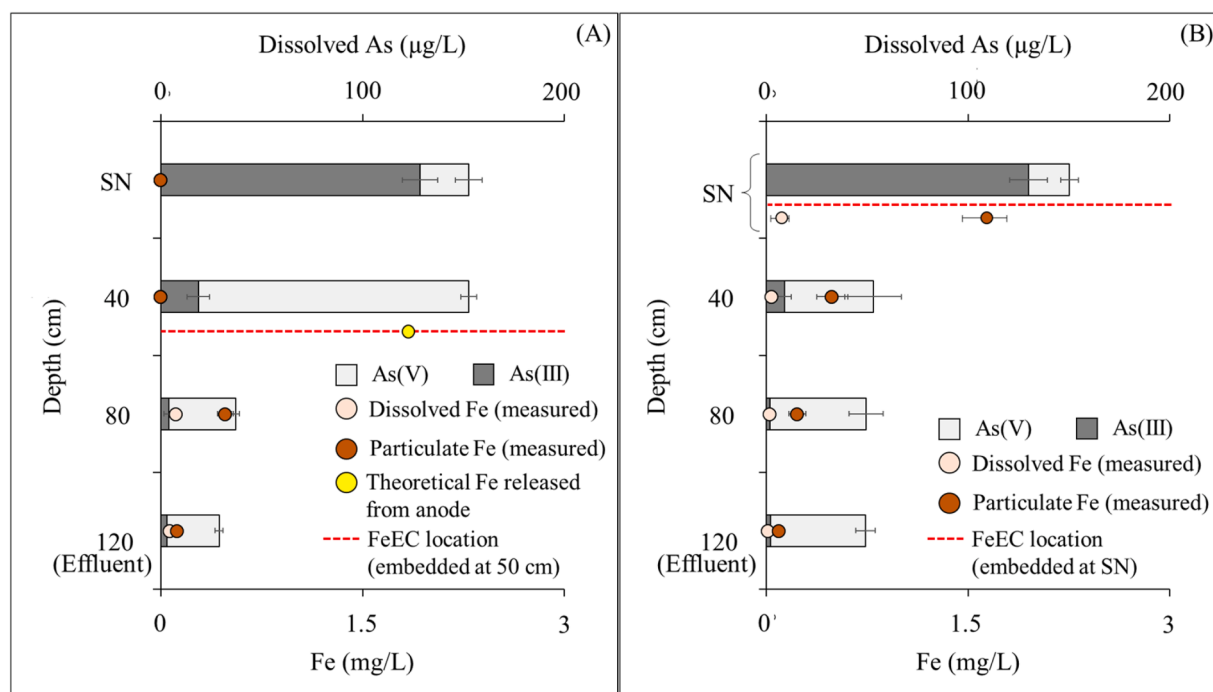
Fig. 3. Fe and As depth profile over the bed height in the biotic embedded-FeEC (A) and supernatant-FeEC (B) filter columns. Tap water spiked with As(III) was dosed as the influent and the columns were operated at CD = 6.4 C/L, flow rate = 3 m/h, and pH = 8.0. The Fe graph shows the concentration of dissolved Fe and particulate Fe that was not filtered by the bed. The yellow circle in (A) indicates the theoretical 1.85 mg/L Fe released by FeEC at CD = 6.4 C/L and flow rate = 3 m/h, as per Eq. (1). SN = supernatant.

system, experiments were conducted by embedding FeEC (depth = 10 cm) in an abiotic bed (duplicate abiotic embedded-FeEC columns) operated with As(V) (Fig. 1(D)). The Fe and As depth profiles during these runs are shown in Fig. 4. The charge dosage (CD), flow rate, and pH were similar to the biotic embedded-FeEC system, except that the influent tap water contained 146±5 µg/L As(V). The results demonstrate that, similar to the biotic embedded-FeEC system in Section 3.2, Fe(II) was released in the abiotic bed, rapidly oxidised to Fe(III)-precipitates, and filtered below the FeEC cell. Within 10 cm and 30 cm of the filter bed (below the FeEC cell), approximately 46 % and 69 % of the released Fe(II) was oxidised and filtered, respectively (considering a theoretical Fe release of 1.85 mg/L). This release of Fe inside the bed led to the removal of the influent As(V) (Fig. 4), with the effluent dissolved As(V) concentration being 21±3.4 µg/L, corresponding to 85 % removal. These findings align with the results of the biotic embedded-FeEC column presented in Section 3.2, where, due to biological As(III) oxidation to As(V), a removal efficiency of 81 % for influent As(III) was observed. This validates the advantage of embedding FeEC in a biological bed, where As(III) removal achieved by embedded-FeEC (under similar Fe dosage) is comparable to that of As(V).

3.4. Enhancing deep-bed infiltration of Fe in embedded-FeEC filter beds

Previous studies have indicated that deep-bed infiltration of Fe(III)-precipitates in sand filters can have a positive effect on As removal (Gude et al., 2018b). However, the rapid filtration observed in the biotic and abiotic embedded-FeEC columns suggested that deep-bed infiltration was not occurring, potentially limiting As removal due to a shorter contact time with the precipitates. To investigate this further, a set of experiments were conducted to assess the impact of varying operational parameters (CD, flow rate, pH) on achieving deep-bed infiltration of the Fe(III)-precipitates in the embedded-FeEC system and the corresponding impact on As removal. The duplicate abiotic embedded-FeEC columns discussed in Section 3.3 were used for these experiments, with the CD,

Fig. 4. Fe and As depth profile over the bed height in the duplicate abiotic embedded-FeEC filter columns. Tap water spiked with As(V) was dosed as the influent and the columns were operated at CD = 6.4 C/L, flow rate = 3 m/h, and pH = 8.0. The Fe graph shows the concentration of dissolved and particulate Fe that was not filtered by the bed. The yellow circle indicates the theoretical 1.85 mg/L Fe released by FeEC at CD = 6.4 C/L and flow rate = 3 m/h, as per Eq. (1). SN = supernatant.

flow rate, or pH being altered. Fig. 5(A), (B), and (C) depict the Fe and As depth profiles in the abiotic embedded-FeEC columns under higher CD (9.4 C/L), higher flow rate (5 m/h), and lower pH (7.0) conditions compared to the reference condition in Section 3.3 (CD = 6.4 C/L, flow rate = 3 m/h, pH = 8.0).

The Fe depth profile observed with a CD of 9.4 C/L was similar to that with 6.4 C/L (Fig. 5(A)). Approximately 79 % of the released Fe (theoretical value of 2.7 mg/L based on Eq. (1)) from the embedded-FeEC was oxidised and filtered within a 30 cm filtration depth below the FeEC cell. However, the effluent As concentration with a CD of 9.4 C/L was 10.7±1.4 µg/L, corresponding to 93 % removal (influent concentration = 156±0.3 µg/L As(V)) (Fig. 5(A)), compared to 85 % removal with a CD of 6.4 C/L (Fig. 4). The higher removal of As(V) with higher CD can be attributed to the increased amount of Fe generated from electrolysis, which is consistent with previous studies conducted in a water matrix in batch mode (van Genuchten et al., 2012; Wan et al., 2011).

Deeper penetration of Fe was observed with a higher flow rate (5 m/h compared to 3 m/h), where the Fe concentration at 10 and 30 cm below the FeEC cell was 1.4 and 0.7 mg/L, respectively, with a flow rate of 5 m/h (Fig. 5(B)). In comparison, with a flow rate of 3 m/h, the corresponding Fe concentrations were 1 and 0.6 mg/L, respectively (Fig. 4). However, a lower removal of As(V) was observed with the flow rate of 5 m/h, where the dissolved As concentration in the effluent was 29±3.4 µg/L, corresponding to 81 % removal (149.7±5 µg/L As(V) influent) (Fig. 5(B)), compared to 85 % with a flow rate of 3 m/h (Fig. 4). This could be attributed to the reduced residence time, resulting in less contact time between As(V) and the released Fe. Furthermore, the higher flow rate also affected the oxidation of Fe(II), as indicated by the higher dissolved Fe concentration (or Fe(II)) of 0.10 mg/L at 5 m/h compared to 0.05 mg/L at 3 m/h, which could have adversely impacted As removal by reducing the availability of Fe(III)-precipitates for As adsorption. Therefore, while an increased flow rate facilitated deep-bed Fe infiltration, the residence time played a crucial role in overall As removal.

Operating the embedded-FeEC system at a lower pH (7.0 compared to 8.0) aimed to decrease the oxidation rate of the released Fe(II) and allow for its deeper distribution within the bed. The Fe depth profile at pH = 7.0 supported this hypothesis, as the dissolved Fe (Fe(II)) concentration at 10 and 30 cm below the FeEC cell was the highest among the different operational conditions (Fig. 5(C)). However, the total Fe concentration in the effluent was the lowest among the different conditions. At 10, 30, and 70 cm below the FeEC cell (effluent), the Fe concentrations were 1.6 (80 % dissolved), 0.7 (67 % dissolved), and 0.2 mg/L at pH = 7.0 (Fig. 5(C)), compared to 1 (13 % dissolved), 0.6 (14 % dissolved), and 0.4 mg/L at pH = 8.0 (Fig. 4), respectively. This indicates that Fe(II) oxidation, precipitation, and filtration occurred at deeper locations within the bed at pH = 7.0, resulting in a higher concentration of Fe at lower depths compared to the experiments at pH = 8.0. The presence of Fe at deeper locations could be likely contributed to the improved As removal at pH = 7.0, where the As concentration in the effluent was 7±1.4 µg/L, corresponding to a 94 % removal (164±6.6 µg/L As(V) influent) (Fig. 5(C)), compared to 85 % at pH = 8.0 (Fig. 4). However, the higher As removal at a lower pH (7.0 over 8.0) can also be attributed to enhanced As(V) adsorption to the Fe(III)-precipitates, as mentioned in previous studies (Dixit and Hering, 2003; Gude et al., 2016). We note here that while As(V) removal improved at lower pH in these experiments, similar trends with pH might not be observed for abiotic experiments performed with initial As(III) since the kinetics of Fe(II) and As(III) co-oxidation decrease significantly with decreasing pH (Garg et al., 2018; King et al., 1995).

3.5. Energy consumption in embedded-FeEC systems

Energy consumption in the abiotic embedded-FeEC columns under different conditions and the supernatant-FeEC column was monitored
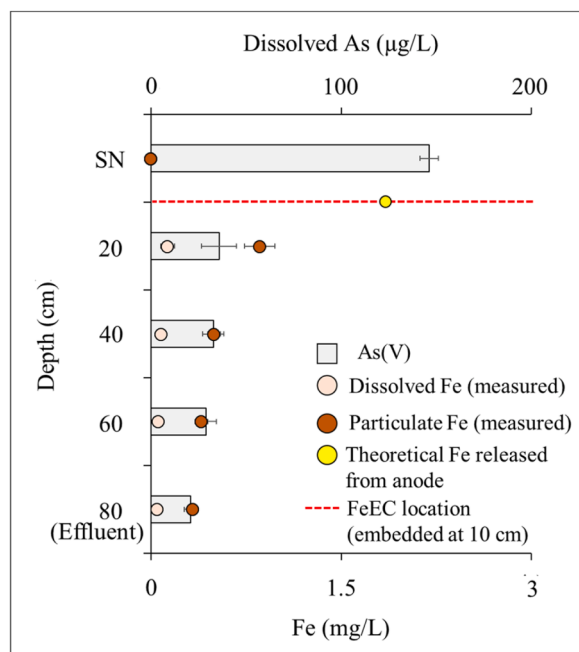
throughout the experiments and is presented as energy consumption per volume of treated water (Wh/m^3), as calculated using Eq. (2). The results obtained under various conditions are shown in Fig. 6.

In the abiotic embedded-FeEC columns operated at CD = 6.4 C/L, flow rate = 3 m/h, and pH = 8.0 or 7.0 (reference or lower pH condition), the initial energy consumption was in the same range, ranging between 12 and 14 Wh/m^3, respectively. However, a higher initial energy consumption was observed for the experiments with a flow rate of 5 m/h (higher flow rate) and CD = 9.4 C/L (higher CD), which were approximately 22 and 30 Wh/m^3, respectively. This difference in the initial consumption value can be explained by the Butler-Volmer relationship (Müller et al., 2019), where an increase in current (I) leads to an increase in the cell potential (E) and, consequently, in the energy consumption. In the case of CD = 9.4 C/L (higher CD), a higher current (I) had to be applied compared to CD = 6.4 C/L. Similarly, for experiments with a flow rate of 5 m/h (higher flow rate), maintaining a constant I/Q (or CD = 6.4 C/L) value as the 3 m/h experiments required a comparatively higher applied current (I) (0.040 A compared to 0.023 A), resulting in an increased cell potential from 8 V (3 m/h) to 12.5 V (5 m/h).

The impact of operating FeEC in a filter bed on cell potential and energy consumption was highlighted in the supernatant-FeEC column. Under constant CD, flow rate, and pH, the supernatant-FeEC column exhibited the lowest initial energy consumption, around 7 Wh/m^3, which was half the value of 14 Wh/m^3 observed in the embedded-FeEC (reference condition) (Fig. 6). This suggests that operating FeEC in a biological filter bed may require more energy compared to supernatant operation. However, achieving efficient As(III) removal similar to the biotic embedded-FeEC column would necessitate a relatively higher CD in the supernatant-FeEC column, resulting in higher energy consumption.

In the embedded-FeEC columns, the cell potential (E) at a constant applied current (I) showed an increasing trend over the course of the experiments. This led to an increase in energy consumption during treatment, as depicted in Fig. 6. For example, in the abiotic embedded-FeEC columns operated under the reference condition, higher CD, higher flow rate, and lower pH, the energy consumption at the end of the experiment increased by 82 %, 92 %, 51 %, and 57 %, respectively, compared to the initial value. This rise in energy consumption over time could be attributed to the accumulation of Fe(III)-precipitates between the electrodes, which increased the cell resistance. Additionally, the accumulation of Fe solids on the electrode surface may have reduced the effective electrode area, resulting in an increase in current density and elevated cell potential (E) and, consequently, increased the energy consumption (Müller et al., 2019). In contrast, the energy consumption over time in the supernatant-FeEC system did not show an increasing trend. This suggests that the cell remained unaffected throughout the experiments, with no changes in cell resistance or effective electrode area.

3.6. Benefits and challenges of embedded-FeEC systems

The findings of this study demonstrate the feasibility of embedding FeEC within a biological filter bed for effective As removal. This embedded-FeEC concept can be utilised to optimise As(III) removal in conventional aeration-filtration processes, where the filter bed is already biologically active for As(III) oxidation. Implementing embedded-FeEC in existing infrastructure eliminates the need for additional construction and allows for efficient As(III) removal without the use of costly chemicals. Adopting a zero-chemical approach resolves issues related to the generation of unwanted by-products, chemical handling and storage, and complex supply chains.

Operating FeEC within a biological bed also enhances As uptake by the released Fe. The As:Fe ratio in the biotic embedded-FeEC column was 0.05 (mol:mol) (considering a theoretical 1.85 mg/L Fe release), while it was 0.04 (mol:mol) (1.73 mg/L Fe release) in the supernatant-

FeEC column. This translates to a lower Fe dosage requirement to achieve the desired As removal, leading to reduced operational costs, sludge generation, backwashing frequency, and environmental impact. However, conducting a Life Cycle Assessment (LCA) for the novel system described in this work is essential to thoroughly evaluate its environmental impact throughout its entire life cycle. This evaluation is crucial for making informed decisions regarding sustainable water management. Therefore, it is recommended to undertake a comprehensive LCA of the biotic embedded-FeEC systems and compare the findings with conventional technologies, such as chemical oxidation and chemical coagulation. This comparative analysis will provide valuable insights for assessing the system's environmental sustainability and guiding future decision-making processes. Moreover, while the biotic embedded-FeEC system removed 81 % of the influent 150 μg/L As(III) and, the removal was not below the WHO guideline value of 10 μg/L, the embedded-FeEC system can be adjusted based on the required level of As removal. One of the main factors that influences As removal during FeEC is the amount of Fe dosed and as observed from batch experiments (Fig. S2), the removal of As can be improved by changing the Fe dosage or CD. Therefore, in the current study or in situations where the As concentration is higher than 150 μg/L, by applying a higher current (I), the Fe dosage can be increased, thereby improving removal efficiency and enabling the attainment of removal levels below 1 μg/L (Dutch drinking water target), as observed in batch experiments (Fig. S2).

It is important to note that embedded-FeEC systems exhibit higher energy consumption compared to operating FeEC in water. This can be considered a drawback since energy consumption significantly impacts operational costs. However, by fine-tuning the operational parameters, the energy consumption of embedded-FeEC systems can be optimised. For example, operating at a relatively higher flow rate (5 m/h) or lower pH (7.0) results in a smaller increase in energy consumption (51 % and 57 % increase, respectively) compared to the reference condition (82 % increase) (Fig. 6). This can be attributed to deep-bed infiltration of the Fe(III)-precipitates under higher flow rate and lower pH conditions (Fig. 5). The deep-bed infiltration phenomenon minimises the accumulation of Fe(III)-precipitates near the electrodes, thereby reducing the impact on cell resistance and effective electrode surface area.

The findings in this study introduce a promising avenue for water treatment by exploring into the idea of embedding and operating FeEC within a biological As(III) oxidising filter bed. However, the system was operated under controlled laboratory conditions using model water that does not accurately reflect natural groundwater conditions. In reality, natural groundwater exhibits variations in pH, the presence of competing ions (e.g., phosphate), fluctuating As concentrations, and other factors known to influence As removal by FeEC. Therefore, although our laboratory findings provided proof of concept, demonstrating the feasibility and advantages of biotic embedded-FeEC systems for As(III) removal, it is strongly recommended to conduct further testing by operating the system with natural groundwater under diverse environmental conditions. This will provide additional insights and validation of the novelty of the proposed system. While the biotic and abiotic embedded-FeEC systems developed in this study were operated for 11 and 7 h, respectively, over three consecutive days, conducting a long-term operational study is crucial to assess their sustained effectiveness, reliability, and environmental impact. This approach ensures informed decision-making for widespread implementation and addresses evolving challenges over time. For example, continuous operation of abiotic embedded-FeEC systems showed an increase in cell resistance and applied voltage (for constant Fe dosage or applied current) over time (Fig. 6). This increase in cell potential can reach the limit of the DC current supplier (30 V in our system), beyond which the system cannot supply the required Fe dosage. Consequently, this reduction in efficiency necessitates a backwash to remove the accumulated Fe(III)-precipitates, thereby reducing the increased cell resistance and restoring the system to its initial performance stage. Moreover, the long-term application of FeEC systems revealed a reduction in the amount of Fe
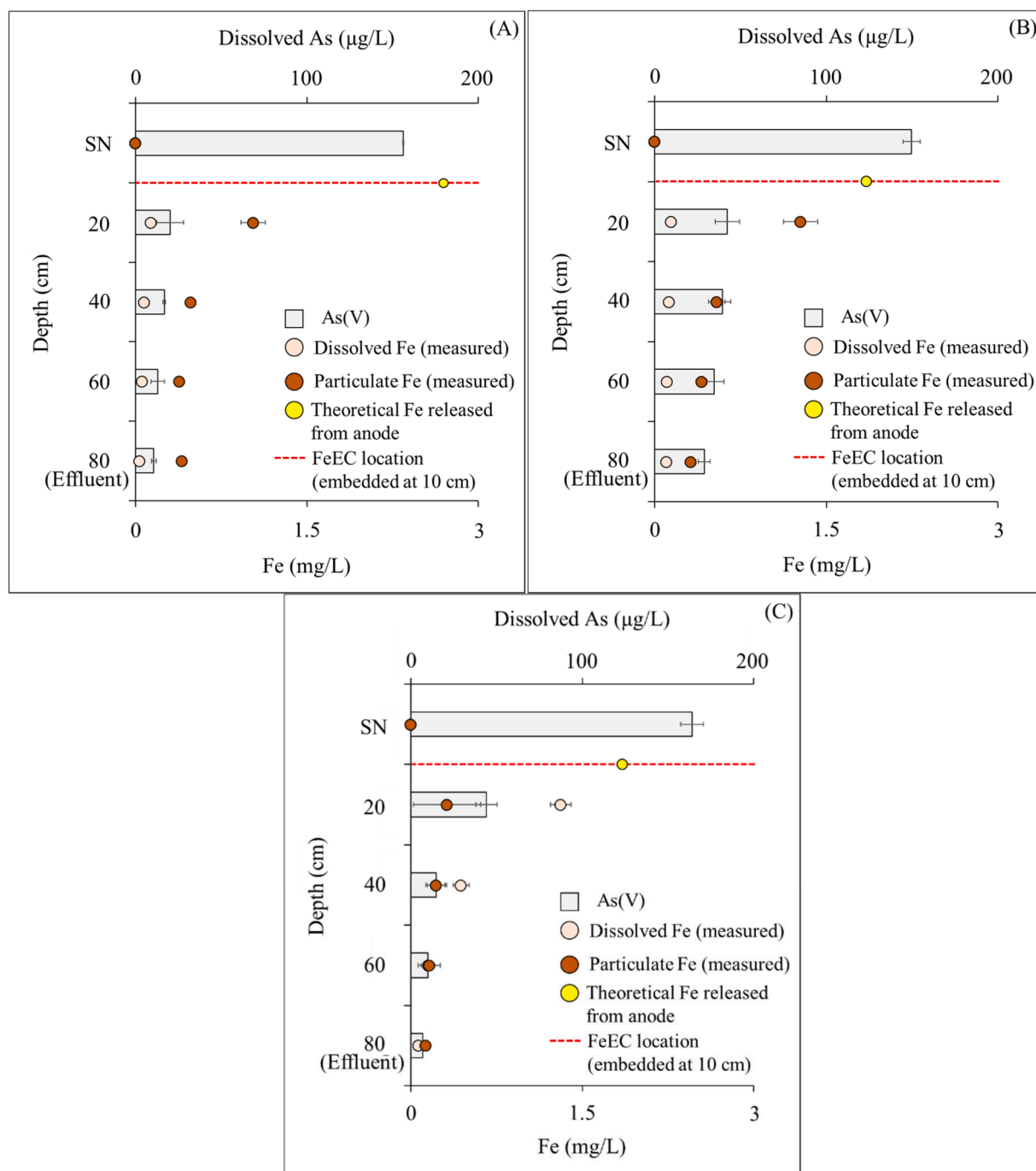
Fig. 5. Fe and As depth profile over the bed height in the duplicate abiotic embedded-FeEC filter columns. Tap water spiked with As(V) was dosed as the influent and the columns were operated at (A) CD = 9.4 C/L, flow rate = 3 m/h, pH = 8.0 (higher CD); (B) CD = 6.4 C/L, flow rate = 5 m/h, pH = 8.0 (higher flow rate); (C) CD = 6.4 C/L, flow rate = 3 m/h, pH = 7.0 (lower pH). The Fe graph shows the concentration of dissolved and particulate Fe that was not filtered by the bed. The yellow circle indicates the theoretical 1.85 or 2.7 mg/L Fe released by FeEC at CD = 6.4 or 9.4 C/L and flow rate = 3 m/h, as per Eq. (1). SN = supernatant.

dosage in the bulk solution for an applied current due to the development of passivation layers on the electrode surface, impacting efficiency (van Genuchten et al., 2016). Therefore, it is recommended to conduct a comprehensive long-term study with embedded-FeEC systems before practical implementation to thoroughly investigate and address potential challenges associated with the system. Identifying and mitigating these challenges will be crucial to ensure the effectiveness and sustainability of this innovative strategy in real-world applications.

4. Conclusion

This study focused on the implementation of horizontally embedded FeEC within a biologically active filter bed for As(III) removal. The performance of this system was compared to FeEC operated in the supernatant water and FeEC embedded in an abiotic filter bed. The results demonstrated that the biotic embedded-FeEC system, where As(III) was first biologically oxidised and then treated with FeEC, achieved a higher As(III) removal efficiency (81 %) compared to operating FeEC in the supernatant water prior to biological oxidation (67 %). Moreover, the As (III) removal in the biotic embedded-FeEC system (81 %) was similar to
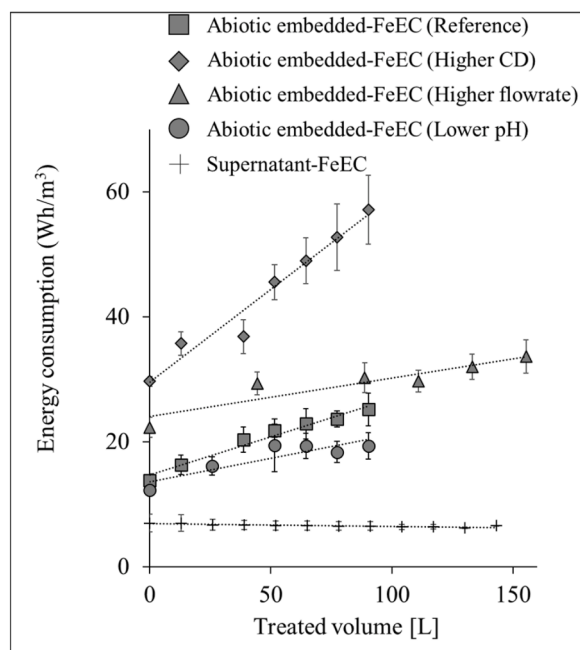
Fig. 6. Energy consumption during the experiments in abiotic embedded-FeEC columns operated under different conditions and the supernatant-FeEC column.

the removal observed when embedded-FeEC was operated in an abiotic bed with As(V)-contaminated water (85 %). However, it should be noted that the embedded-FeEC systems exhibited higher energy requirements compared to operating FeEC in the supernatant water. The efficiency of As removal and energy consumption in these embedded-FeEC systems was further influenced by the deep-bed infiltration of Fe(III)-precipitates, which can be controlled by adjusting operational parameters such as flow rate and pH. Nevertheless, the novelty of the embedded-FeEC system lies in leveraging biological As(III) oxidation within rapid sand filter beds of conventional aeration-filtration systems to effectively remove oxidised As(V) within the bed, without the need for chemicals or significant additional infrastructure.

Declaration of competing interest

The authors declare that they have no known competing financial interests or personal relationships that could have appeared to influence the work reported in this paper.

Data availability

Data will be made available on request.

Supplementary materials

Supplementary material associated with this article can be found, in the online version, at doi:10.1016/j.watres.2024.121233.

References

Ahmad, A., Cornelissen, E., van de Wetering, S., van Dijk, T., van Genuchten, C., Bundschuh, J., van der Wal, A., Bhattacharya, P., 2018. Arsenite removal in groundwater treatment plants by sequential Permanganate–Ferric treatment. J. Water. Process. Eng. 26, 221–229. https://doi.org/10.1016/J.JWPE.2018.10.014.

Alka, S., Shahir, S., Ibrahim, N., Ndejiko, M.J., Vo, D.V.N., Manan, F.A., 2021. Arsenic removal technologies and future trends: A mini review. J. Clean. Prod. 278 https://doi.org/10.1016/J.JCLEPRO.2020.123805.

Amrose, S.E., Bandaru, S.R.S., Delaire, C., van Genuchten, C.M., Dutta, A., DebSarkar, A., Orr, C., Roy, J., Das, A., Gadgil, A.J., 2014. Electro-chemical arsenic remediation: Field trials in West Bengal. Sci. Total Environ. 488 (1), 539–546. https://doi.org/10.1016/j.scitotenv.2013.11.074. -489.

Bandaru, S.R.S., Roy, A., Gadgil, A.J., van Genuchten, C.M., 2020. Long-term electrode behavior during treatment of arsenic contaminated groundwater by a pilot-scale iron electrocoagulation system. Water. Res. 175, 115668 https://doi.org/10.1016/j.watres.2020.115668.

Delaire, C., Amrose, S., Zhang, M., Hake, J., Gadgil, A., 2017. How do operating conditions affect As(III) removal by iron electrocoagulation? Water. Res. 112, 185–194. https://doi.org/10.1016/j.watres.2017.01.030.

Dixit, S., Hering, J.G., 2003. Comparison of Arsenic(V) and Arsenic(III) Sorption onto Iron Oxide Minerals: Implications for Arsenic Mobility. Environ. Sci. Tech. 37 (18), 4182–4189. https://doi.org/10.1021/ES030309T.

Garg, S., Jiang, C., Waite, T.D., 2018. Impact of pH on Iron Redox Transformations in Simulated Freshwaters Containing Natural Organic Matter. Environ. Sci. Tech. 52 (22), 13184–13194. https://doi.org/10.1021/ACS.EST.8B03855/ASSET/IMAGES/LARGE/ES-2018-03855R_0006.JPEG.

Gude, J.C.J., Joris, K., Huysman, K., Rietveld, L.C., van Halem, D., 2018a. Effect of supernatant water level on As removal in biological rapid sand filters. Water. Res. X. 1 https://doi.org/10.1016/j.wroa.2018.100013.

Gude, J.C.J., Rietveld, L.C., van Halem, D., 2018b. As (III) removal in rapid filters: Effect of pH, Fe (II)/Fe (III), filtration velocity and media size. Water. Res. 147, 342–349. https://doi.org/10.1016/j.watres.2018.10.005.

Gude, J.C.J., Rietveld, L.C., van Halem, D., 2016. Fate of low arsenic concentrations during full-scale aeration and rapid filtration. Water. Res. 88, 566–574. https://doi.org/10.1016/j.watres.2015.10.034.

Gude, J.C.J., Rietveld, L.C., van Halem, D., 2018c. Biological As(III) oxidation in rapid sand filters. J. Water. Process. Eng. 21, 107–115. https://doi.org/10.1016/j.jwpe.2017.12.003.

Hug, S.J., Leupin, O., 2003. Iron-catalysed oxidation of Arsenic(III) by oxygen and by hydrogen peroxide: pH-dependent formation of oxidants in the Fenton reaction. Environ. Sci. Tech. 37 (12), 2734–2742. https://doi.org/10.1021/es026208x.

Jackman, T.A., Hughes, C.L., 2010. Formation of Trihalomethanes in Soil and Groundwater by the Release of Sodium Hypochlorite. Ground. Water. Monit. Remediat. 30 (1), 74–78. https://doi.org/10.1111/j.1745-6592.2009.01266.x.

Kapaj, S., Peterson, H., Liber, K., Bhattacharya, P., 2006. Human health effects from chronic arsenic poisoning - A review. J. Environ. Sci. Health Part A Toxic/Haz. Subs. Environ. Eng. 41 (10), 2399–2428. https://doi.org/10.1080/10934520600873571.

Katsoyiannis, I.A., Zouboulis, A.I., 2004. Application of biological processes for the removal of arsenic from groundwaters. Water. Res. 38 (1), 17–26. https://doi.org/10.1016/j.watres.2003.09.011.

King, D.W., Lounsbury, H.A., Millero, F.J., 1995. Rates and Mechanism of Fe(II) Oxidation at Nanomolar Total Iron Concentrations. Environ. Sci. Tech. 29 (3), 818–824. https://doi.org/10.1021/ES00003A033.

Kowalski, K.P., 2014. Advanced Arsenic Removal Technologies Review. Chemistry of Advanced Environmental Purification Processes of Water: Fundamentals and Applications 285–337. https://doi.org/10.1016/B978-0-444-53178-0.00008-0.

Kumpiene, J., Engström, K., Pinedo Taquia, A., Carabante, I., Bjuhr, J., 2023. Arsenic immobilisation in soil using electricity-induced spreading of iron in situ. J. Environ. Manage. 325 https://doi.org/10.1016/J.JENVMAN.2022.116467.

Lytle, D.A., Chen, A.S., Sorg, T.J., Phillips, S., French, K., 2007. Microbial As(III) oxidation in water treatment plant filters. J. Am. Water. Works Assoc. 99 (12), 72–86. https://doi.org/10.1002/j.1551-8833.2007.tb08108.x.

Mollah, M.Y.A., Morkovsky, P., Gomes, J.A.G., Kesmez, M., Parga, J., Cocke, D.L., 2004. Fundamentals, present and future perspectives of electrocoagulation. J. Hazard. Mater. 114 (1–3), 199–210. https://doi.org/10.1016/j.jhazmat.2004.08.009.

Müller, S., Behrends, T., van Genuchten, C.M., 2019. Sustaining efficient production of aqueous iron during repeated operation of Fe(0)-electrocoagulation. Water. Res. 155, 455–464. https://doi.org/10.1016/j.watres.2018.11.060.

Roberts, L.C., Hug, S.J., Ruettimann, T., Billah, M., Khan, A.W., Rahman, M.T., 2004. Arsenic Removal with Iron(II) and Iron(III) in Waters with High Silicate and Phosphate Concentrations. Environ. Sci. Tech. 38 (1), 307–315. https://doi.org/10.1021/es0343205.

Roy, M., van Genuchten, C.M., Rietveld, L., van Halem, D., 2020. Integrating biological As(III) oxidation with Fe(0) electrocoagulation for arsenic removal from groundwater. Water. Res. 188, 116531 https://doi.org/10.1016/j.watres.2020.116531.

Sodhi, K.K., Kumar, M., Agrawal, P.K., Singh, D.K., 2019. Perspectives on arsenic toxicity, carcinogenicity and its systemic remediation strategies. Environ. Tech. Innov. 16 https://doi.org/10.1016/J.ETI.2019.100462.

Sorlini, S., Gialdini, F., 2010. Conventional oxidation treatments for the removal of arsenic with chlorine dioxide, hypochlorite, potassium permanganate and monochloramine. Water. Res. 44 (19), 5653–5659. https://doi.org/10.1016/j.watres.2010.06.032.

Steinmaus, C., Ferreccio, C., Acevedo, J., Yuan, Y., Liaw, J., Durán, V., Cuevas, S., García, J., Meza, R., Valdés, R., Valdés, G., Benítez, H., Van Der Linde, V., Villagra, V., Cantor, K.P., Moore, L.E., Perez, S.G., Steinmaus, S., Smith, A.H., 2014. Increased lung and bladder cancer incidence in adults after in utero and early-life arsenic exposure. Cancer Epidemiology, Biomarkers & Prevention : A Publication of the American Association for Cancer Research, Cosponsored by the American Society of Preventive Oncology 23 (8), 1529–1538. https://doi.org/10.1158/1055-9965.EPI-14-0059.

van Genuchten, C.M., Bandaru, S.R.S., Surorova, E., Amrose, S.E., Gadgil, A.J., Peña, J., 2016. Formation of macroscopic surface layers on Fe(0) electrocoagulation electrodes during an extended field trial of arsenic treatment. Chemosphere 153, 270–279. https://doi.org/10.1016/j.chemosphere.2016.03.027.

van Genuchten, C.M., Behrends, T., Dideriksen, K., 2019. Emerging investigator series: Interdependency of green rust transformation and the partitioning and binding mode of arsenic. Environ. Sci. 21 (9), 1459–1476. https://doi.org/10.1039/C9EM00267G.

van Genuchten, C.M., Behrends, T., Kraal, P., Stipp, S.L.S., Dideriksen, K., 2018. Controls on the formation of Fe(II,III) (hydr)oxides by Fe(0) electrolysis. Electrochim. Acta 286, 324–338. https://doi.org/10.1016/j.electacta.2018.08.031.

van Genuchten, C.M., Behrends, T., Stipp, S.L.S., Dideriksen, K., 2020. Achieving arsenic concentrations of <1 μg/L by Fe(0) electrolysis: The exceptional performance of magnetite. Water. Res. 168, 115170 https://doi.org/10.1016/j.watres.2019.115170.

van Genuchten, C.M., Dalby, K.N., Ceccato, M., Stipp, S.L.S., Dideriksen, K., 2017. Factors affecting the Faradaic efficiency of Fe(0) electrocoagulation. J. Environ. Chem. Eng. 5 (5), 4958–4968. https://doi.org/10.1016/J.JECE.2017.09.008.

van Genuchten, Case M., Addy, S.E.A., Peña, J., Gadgil, A.J, 2012. Removing arsenic from synthetic groundwater with iron electrocoagulation: An Fe and As K-edge EXAFS study. Environ. Sci. Tech. 46 (2), 986–994. https://doi.org/10.1021/es201913a.

van Genuchten, Case M., Peña, J., Amrose, S.E., Gadgil, A.J, 2014. Structure of Fe(III) precipitates generated by the electrolytic dissolution of Fe(0) in the presence of groundwater ions. Geochim. Cosmochim. Acta 127, 285–304. https://doi.org/10.1016/J.GCA.2013.11.044.

Wan, W., Pepping, T.J., Banerji, T., Chaudhari, S., Giammar, D.E., 2011. Effects of water chemistry on arsenic removal from drinking water by electrocoagulation. Water. Res. 45 (1), 384–392. https://doi.org/10.1016/j.watres.2010.08.016.

World Health Organization, 2004. Guidlines For Drinking-water Quality, 3rd ed., 1. World Health Organization, Geneva, Switzerland. Recommendations.

Yang, L., Li, X., Chu, Z., Ren, Y., Zhang, J., 2014. Distribution and genetic diversity of the microorganisms in the biofilter for the simultaneous removal of arsenic, iron and manganese from simulated groundwater. Bioresour. Technol. 156, 384–388. https://doi.org/10.1016/J.BIORTECH.2014.01.067.